ACS APPLIED MATERIALS & INTERFACES

Research Article

www.acsami.org

# Preparation of Three-Dimensional Graphene Oxide–Polyethylenimine Porous Materials as Dye and Gas Adsorbents

Zhu-Yin Sui, Yi Cui, Jian-Hua Zhu, and Bao-Hang Han*

National Center for Nanoscience and Technology, Beijing 100190, China

Supporting Information

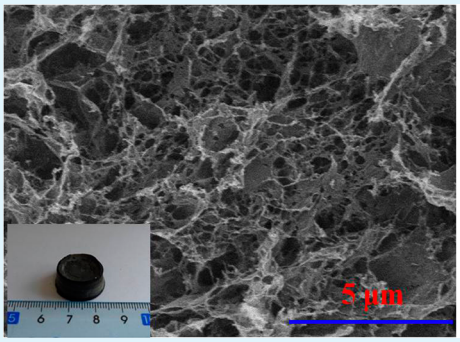


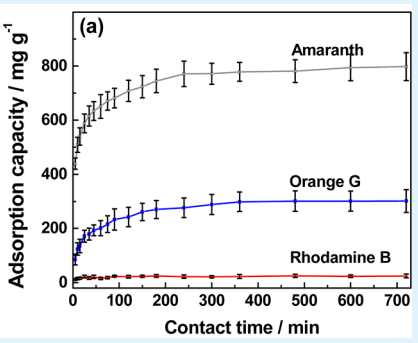


**ABSTRACT:** We report a facile method for the fabrication of three-dimensional (3D) porous materials via the interaction between graphene oxide (GO) sheets and polyethylenimine (PEI) with high amine density at room temperature under atmospheric pressure without stirring. The structural and physical properties of GO–PEI porous materials (GEPMs) are investigated by scanning electron microscopy, X-ray diffraction, thermogravimetric analysis, and nitrogen adsorption–desorption measurement and their chemical properties are analyzed by X-ray photoelectron spectroscopy, infrared spectroscopy, and Raman spectroscopy. GEPMs possess low density and hierarchical morphology with large specific surface area, and big pore volume. Furthermore, the as-prepared 3D porous materials show an excellent adsorption capacity for acidic dyes on the basis of the pore-rich and amine-rich graphene structure. GEPMs exhibit an extremely high adsorption capacity for amaranth (800 mg $g^{-1}$), which are superior to other carbon materials. In addition, GEPMs also exhibit good adsorption capacity for carbon dioxide (11.2 wt % at 1.0 bar and 273 K).

**KEYWORDS:** *graphene oxide, graphene, adsorption, porous materials*

## INTRODUCTION

Graphene, a two-dimensional (2D) single-layer sheet of $sp^2$-hybridized conjugated carbon atoms, has attracted great interest for its potential use in various applications, such as hydrogen storage,[1−6] carbon dioxide capture,[7−10] and electrode material in electrochemical energy devices.[11−16] Graphene oxide (GO), an amazing derivative of graphene, possesses various reactive functional groups, such as hydroxyl, epoxy, and carboxylic groups.[17] Recently, GO-based materials have attracted intense interest for energy- and environment-related applications because of their multifunctional flexibility.[7,18−20]

2D sheet assemblies have drawn considerable concern for both fundamental researches and applications, since they provide direct bridges between nanometer-scale and the macroscale system.[21] Assembling individual graphene or GO sheets into macroscopic porous monolithic materials is an essential step to achieve a variety of potential applications of graphene and its derivatives.[21] The assembled structures possess novel physiochemical properties that are different from individual components and the bulk materials. Recently, there have been many studies focusing on exploring the fabrication of three-dimensional (3D) architectures of graphene or its derivatives to expand its practical applications. Shi et al. reported the fabrication of graphene architecture by hydrothermal processing, and the obtained hydrogels with 97.4 wt % water possess excellent electrical and mechanical properties.[22] However, it requires high pressure and high temperature to form the hydrogels, which is difficult to proceed at a large scale. The preparation of graphene aerogel was first reported by Worsley et al. through the sol–gel polymerization of resorcinol and formaldehyde in aqueous GO dispersion, and the 3D macroassembly of graphene sheets shows a large surface area and high electrical conductivity.[23] A versatile, ultralight, 3D nitrogen-doped graphene framework was prepared by Qu et al. through the hydrothermal processing and pyrolysis of GO/pyrrole composite.[24] However, to obtain the graphene aerogel and nitrogen-doped graphene framework, the above-mentioned composite materials have to be pyrolyzed at a high temperature. In addition, chemical or physical cross-linkers, such as DNA molecules,[25] metal ions,[26,27] and polymers[28−31] are employed

Received: July 4, 2013
Accepted: August 26, 2013
Published: August 26, 2013

  

to assemble graphene and its derivatives into monolithic structures. Therefore, an effective and environmentally friendly strategy to prepare 3D porous materials with a large specific surface area is still needed.

In the past few years, polyethylenimine (PEI) has received tremendous attention as versatile building blocks for the construction of adsorbents as a result of its high amine density and accessible primary amine sites on chain ends.[32−36] The interaction between PEI and silica has recently been used to form PEI/silica composite materials that exhibit an excellent $CO_2$ adsorption capacity.[32,37−41] Similarly, GO consists of oxygen functional groups on their basal planes and edges, therefore, GO could show high affinity to amines or amine-containing molecules. If PEI polymers attach to its layers, the residual amine groups can exhibit good adsorption capacity for acidic gas or anionic materials, such as polyanions and negatively charged organic or inorganic solids. Although PEI polymers can easily interact with the oxygenated groups of GO sheets, synthesizing porous GO−PEI materials with large specific surface area is still a great challenge. 3D GO−PEI porous materials have not been reported as versatile adsorbents previously. This work is anticipated to open a possibility in integrating GO and PEI with high amine density for obtaining high-performance porous materials in dealing with environmental protection issues.

In this paper, we demonstrate a facile approach to the fabrication of lightweight GO-based porous materials with 3D interconnected networks under mild conditions. PEI was chosen as the amine source and cross-linker because of its high amine density. The GO−PEI porous materials (GEPMs) with bulk densities in the range of 0.02−0.03 g $cm^{-3}$ show hierarchical morphology with large specific surface area and big pore volume. Furthermore, the 3D porous materials possess an excellent adsorption capacity for acidic dyes and $CO_2$. These results demonstrate the great promise of GEPMs as new super adsorption materials for high-efficiency sorbent applications. Our work also offers the inspiration for preparing other multifunctional porous monolithic materials based on graphene and its derivatives.

## EXPERIMENTAL SECTION

**Materials.** Natural flake graphite with an average particle diameter of 20 $\mu$m (99 wt % purity) was obtained from Yingshida graphite Co. Ltd., Qingdao, China. Sulfuric acid (98 wt %), hydrogen peroxide (30 wt %), sodium hydroxide, sodium nitrate, amaranth, rhodamine B, cetyl trimethylammonium bromide (CTAB), and ethanol are of analytical grade and were purchased from Beijing Chemical Reagents Company. Orange G was purchased from Jinke Research Institute of Fine Chemicals (Tianjin, China). Chemical structures of amaranth, orange G, and rhodamine B are shown in Figure S1 (Supporting Information). PEI ($M_w \approx 800$ g $mol^{-1}$) was purchased from Sigma-Aldrich Company. All chemicals were used without further purification. Ultrapure water (18 MΩ cm) used in all experiments was produced by a Millipore-ELIX water purification system.

**Preparation of 3D Porous GO−PEI Materials.** Aqueous GO dispersion was prepared by a modified Hummers' method using the natural flake graphite.[42,43] Aqueous GO dispersion was sonicated for 60 min prior to use. The pH value of the as-prepared GO dispersion (10 mg $mL^{-1}$) was adjusted to 8.0 by adding an appropriate amount of aqueous sodium hydroxide solution (0.1 M) dropwise. To prepare GEPMs (e.g., weight ratio = 1:3), GO dispersion (10 mg $mL^{-1}$, 2.5 mL) at pH = 8.0 was mixed with aqueous PEI solution (30 mg $mL^{-1}$, 2.5 mL). Then, the mixture was stirred and sonicated for about 1 min. The gel precursor was stored at 25 °C for 24 h to obtain well formed GO−PEI hydrogel. Then, the resulting hydrogel was immersed in a large amount of ultrapure water thoroughly to remove sodium hydroxide and unattached PEI. Finally, GEPMs were prepared by freeze-drying under vacuum (less than 20 Pa) for 24 h. GEPMs with different feeding ratios were also prepared by the similar method. The products are named as GEPM-1, GEPM-2, GEPM-3, GEPM-4, and GEPM-5 with different feeding ratio of PEI to GO (weight ratio = 3:1, 2:1, 1:1, 1:3, and 1:6), respectively. The bulk densities of the GEPMs have been calculated by the mass of GEPM divided by its volume.

GO and hydrothermal reduced graphene (HTG) porous materials were prepared as control samples by freeze-drying of aqueous GO dispersion and HTG hydrogel. HTG hydrogel was prepared by heating homogeneous aqueous GO dispersion (2 mg $mL^{-1}$) sealed in a Teflon-lined stainless-steel autoclave at 180 °C for 12 h.

**Dye Adsorption Experiments.** Two acidic dyes (amaranth and orange G) and one basic dye (rhodamine B) were employed to investigate the adsorption behavior of the as-prepared GEPMs. In a typical experiment, the as-prepared GEPMs (10 mg) was added into aqueous dye solution (200 mL of 50 mg $L^{-1}$), followed by stirring in a shaking incubator at 25 °C. At predetermined time intervals, 2 mL of the mixture was taken out and the dye concentration remaining in the mixture was measured after centrifugation at 10000 rpm for 5 min. The concentration of dye was determined through UV−Vis spectrometer at the maximum absorbance of each dye (554, 478, and 522 nm for rhodamine B, orange G, and amaranth, respectively). The amount of dye absorbed on absorbents at time $t$, $q_t$ (mg $g^{-1}$), was calculated using the following equation:

$$q_t = \frac{(C_0 - C_t) \times V}{m} \quad (1)$$

where $C_0$ and $C_t$ (mg $L^{-1}$) are the concentration of dye initially and at time $t$, respectively, $V$ is the volume of dye solution (L), and $m$ is the mass of adsorbent used (g). The measurements were repeated for each sample, and the average value was used as the final result.

The pseudo-first-order kinetic equation is presented as:

$$\log(q_e - q_t) = \log q_e - \frac{k_1}{2.303} t \quad (2)$$

The pseudo-second-order kinetic equation is given as

$$\frac{t}{q_t} = \frac{1}{k_2 q_e^2} + \frac{t}{q_e} \quad (3)$$

where $q_e$ and $q_t$ are the dye amount adsorbed with samples at equilibrium and at time $t$, respectively; $k_1$ and $k_2$ represent the pseudo-first-order ($min^{-1}$) and pseudo-second-order (g $mg^{-1}$ $min^{-1}$) rate constant, respectively.

CTAB was chosen as the regenerant to investigate the desorption behavior of the loaded dye within the GEPMs. The details were described as follows: First, the mixtures of the dye and GEPMs were filtered with a large amount of water. Then the adsorbent containing the absorbed dye was added into ultrapure water (250 mL) and CTAB (200 mg) was added into above suspension to remove the dye from the applied adsorbent.

**Instrumental Characterization.** Nitrogen sorption and carbon dioxide sorption isotherms were obtained with a Micromeritics TriStar II 3020 surface area and porosity analyzer. Nitrogen sorption analysis was measured at 77 K, and the obtained nitrogen sorption isotherms were evaluated to give pore properties such as specific surface area, pore size distribution, and total pore volume. All data were averaged from two or three measurements. Before measurement, the sample was degassed under vacuum at 80 °C for 12 h. The carbon dioxide adsorption isotherms of the samples were collected at 273 K. The measurements were repeated for each sample, and the average value was used as the final result. Scanning electron microscopy (SEM) observations were carried out using a Hitachi S-4800 microscope (Hitachi Ltd., Japan) at an accelerating voltage of 5−10 kV. X-ray photoelectron spectroscopy (XPS) data were obtained with an ESCALab220i-XL electron spectrometer (VG Scientific Ltd., U.K.) using 300 W Al $K_\alpha$ radiation. The base pressure was about $3 \times 10^{-9}$ mbar. Thermal gravimetric analysis (TGA) was performed on a Pyris

Diamond thermogravimetric/differential thermal analyzer by heating the samples to 800 °C at 10 °C $min^{-1}$ in the atmosphere of nitrogen. X-ray diffraction (XRD) patterns of the samples were measured from 4° to 60° by a Philips X'Pert PRO X-ray diffraction instrument. Infrared (IR) spectra were recorded in KBr pellets using a Spectrum One Fourier transform infrared (FTIR) spectrometer (Perkin–Elmer Instruments Co. Ltd., U.S.A.). Raman spectra were recorded with a Renishaw inVia Raman spectrometer (Renishaw plc, U.K.). The laser excitation was provided by a regular model laser operating at 514 nm. The ultraviolet–visible (UV–vis) spectra were recorded with a Perkin–Elmer Lamda 950 UV–Vis–NIR spectrophotometer.

## RESULTS AND DISCUSSION

GO was prepared by a modified Hummers' method using the natural flake graphite as our previous reports.[44−47] GO sheets can be easily dispersed in water to form a stable colloidal dispersion owing to the presence of various hydrophilic oxygenated functional groups (hydroxyl, carboxyl, and epoxy groups) on the surface and edge of the GO sheets.[17] These oxygenated functional groups can form hydrogen bonding and electrostatic interaction with other molecules under appropriate conditions.[28,29]

In this work, PEI with high amine density has been chosen as cross-linking agent to interact with GO sheets in water and GO–PEI hydrogel can be fabricated under mild conditions via strong interaction between PEI polymers and GO sheets. Before applying the GO dispersion, its pH was adjusted to ∼8 by using an appropriate amount of aqueous sodium hydroxide solution with a concentration of 0.1 M. Applying the GO dispersion of a lower pH value will not yield homogeneous gel, which may mainly result from the fast cross-linking between amino groups of PEI polymers and oxygen-containing groups of GO sheets. As shown in Figure 1, aqueous GO dispersion

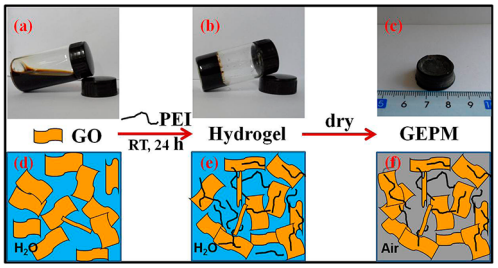


**Figure 1.** Illustration of the preparation process of the GO–PEI porous materials (GEPMs): digital pictures of aqueous GO dispersion (a), GO–PEI hydrogel (b), and GEPM (c) and schematic diagram of aqueous GO dispersion (d), GO–PEI hydrogel (e), and GEPM (f).

mixed with PEI solution at 25 °C for 24 h to get well-formed GO–PEI gel. The resulting GO–PEI gel was immersed in a great amount of ultrapure water, followed by freeze-drying at −50 °C to avoid destruction of the 3D structure and obtain the GEPMs.

GEPMs possess a low density in the range of 0.02–0.03 g $cm^{-3}$, which is comparable to those of monolithic graphene-based materials (0.01–0.1 g $cm^{-3}$).[48−50] The low density of GEPMs could be ascribed to the rich open-pore structures interpenetrating the skeleton of GO sheets (Figure 2a). It can be seen from SEM images that the GEPMs exhibit a well-defined 3D porous network structure composed of a large amount of interconnected macropores. The porous properties of the as-prepared GEPMs were also characterized by the nitrogen adsorption–desorption measurement (Figure 2b). The nitrogen adsorption–desorption isotherm of GEPM-3 reveals a Brunauer–Emmett–Teller (BET) specific surface area of 476 $m^2$ $g^{-1}$, which is higher than that of nitrogen-doped graphene framework (280 $m^2$ $g^{-1}$)[24] and comparable to that of monolithic graphene aerogels (512 $m^2$ $g^{-1}$),[48] suggesting the prominent porous structure of the lightweight GEPMs in consistence with SEM observation. For pure GO sample without the cross-linking of PEI polymers, its BET specific surface area was 31 $m^2$ $g^{-1}$, which is close to that reported preciously,[7,47] indicating the severe stacking of GO sheets during the process of drying. The specific surface area data of GEPMs with different feeding ratios of GO and PEI were determined (Figure S2, Supporting Information). The specific surface area of the GEPMs increases with the increase in the amount of PEI and reaches its maximum when the feeding ratio is 1:1 (GO:PEI), while the specific surface area of GEPMs drops down with the further increase in the amount of PEI. The enhancement of specific surface area could be ascribed to the appropriate PEI polymers covering onto the surface of GO sheets, which effectively prevent GO sheets from stacking. However, when the amount of PEI is too much, only part of PEI polymers takes effect. So the specific surface area of GEPMs decreases as the PEI contents increase. Figure S3 and Table S1 (Supporting Information) summarizes the porous properties of GEPMs obtained from nitrogen sorption measurements, from which it can be seen that the BET specific surface area ($S_{BET}$) and the total pore volume ($V_{total}$) of the obtained 3D porous materials are in the range of 200–480 $m^2$ $g^{-1}$ and 0.6–1.3 $cm^3$ $g^{-1}$, respectively.

XRD patterns shown in Figure 3 further show that PEI polymers were attached onto the GO sheets. Compared with GO, we observed an obvious increase in the interlayer spacing in the GEPM-4, GEPM-3, and GEPM-2, from 0.78 (11.3°) to 1.05 (8.4°) to 1.39 (6.4°) to 1.56 nm (5.7°), indicating successful introduction of PEI polymers between the GO sheets. It has been reported that the diffraction peaks in XRD patterns become weak or even disappear if GO is cross-linked at either edge or side of the sheets and its regular stacks are destroyed.[51,52] With the further increase of PEI polymers, no obvious peaks can be observed in GEPM-1, indicating that the introduction of PEI polymers successfully prevented the restacking of GO sheets.

XPS was used to analyze the chemical composition of GO and GEPMs. As shown in Figure 4a, three prominent peaks centered at 285, 532, and 400 eV correspond to the $C_{1s}$ (67.4 at. %), $O_{1s}$ (15.3 at. %), and $N_{1s}$ (17.3 at. %), respectively. The high-resolution $N_{1s}$ spectrum reveals the presence of amide (398.6 eV), amine (399.5 eV), and $N^+$ species (401.5 eV), suggesting the presence of PEI polymers in the GEPMs, either in their original amine forms or in grafted forms through the amide covalent bonding to the GO sheets.[53,54] The IR spectra of GO and GEPM-1 samples provide further evidence for the presence of PEI, where significant difference can be observed (Figure 4c). Compared with GO, we found slight increases in the two peaks at 2854 and 2921 $cm^{-1}$ assignable to symmetric and asymmetric stretching modes of $CH_2$ of the PEI chains,[55,56] and obvious decrease in the peak at 1731 $cm^{-1}$ attributed to C=O of COOH. This infers that most carbonyl moieties might convert into amides, which results in appearance of a new band at 1650 $cm^{-1}$.[54] In addition, new bands at 1450 $cm^{-1}$ (C–N stretching vibration) and 1582 $cm^{-1}$ (N–H bending vibration) appear in GEPM-1, also reflecting the introduction of PEI. These changes in FTIR and XPS spectra confirm the

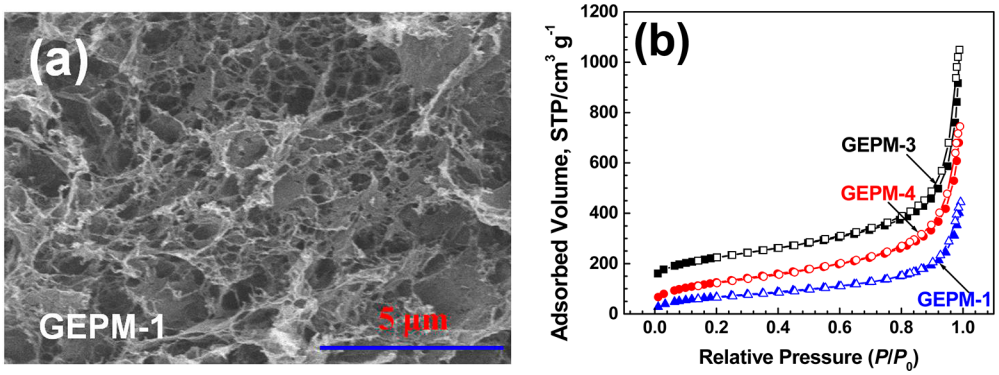


**Figure 2.** (a) SEM image of the obtained GO–PEI porous material (GEPM) and (b) typical nitrogen sorption isotherms of GEPM-1, GEPM-3, and GEPM-4 (solid symbols for adsorption and empty symbols for desorption). The isotherm of GEPM-3 has been offset by 100 units for the purpose of clarity.

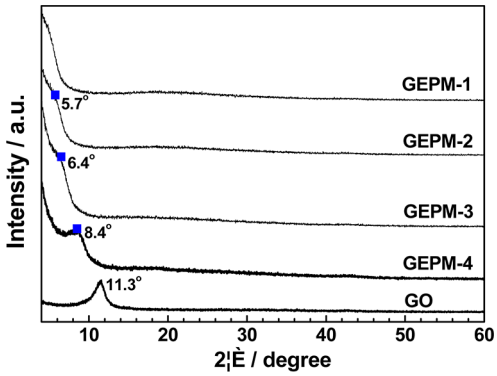


**Figure 3.** Wide-angle X-ray diffraction patterns of the GO–PEI porous materials (GEPMs) (solid square for shoulder peak position).

presence of PEI polymers on the GO surface and some PEI chains are covalently linked to the GO surface by amide bonds. Scheme 1 demonstrates the interaction between GO sheets and PEI polymers.

The thermal stability of GO and GEPMs was studied by TGA. Figure 4d shows the weight loss of the samples as a function of temperature in nitrogen atmosphere. GO is thermally unstable and its mass loss at around 230 °C was about 40%, which can be ascribed to the decomposition of labile oxygen-containing functional groups.[55,57,58] Compared with GO, GEPMs show a slighter mass loss at around 230 °C, indicating the slight reduction of GO during the introduction of PEI, which is in accordance with the IR results. The weight loss of the GEPMs at 245–800 °C could primarily result from the thermal decomposition of PEI[59] and the contribution from the oxygenated groups of GO sheets. If deducting the possible removal (22 wt %) of oxygenated groups of GO at 245–800 °C during the thermal decomposition of GEPMs, the PEI content in GEPMs was calculated to be in the range of 25–40 wt %. According to the PEI content and BET specific surface area, the amine densities in GEPMs were estimated to be 8–22 ethylenimine (EI) units per square nanometer (molecular weight of EI unit is 43)

It is well-known that Raman spectroscopy is a powerful tool to characterize carbonaceous materials. The common characteristic peaks, *D*-band (1352 $cm^{-1}$) and *G*-band (1592 $cm^{-1}$), correspond to $sp^3$ carbon atoms of the defect structure and $sp^2$-hybridized carbon atoms from the aromatic structure, respectively.[5] The Raman spectra (Figure 5) of GEPM samples show two prominent peaks at the same range compared with that of GO, indicating the existence of GO in GEPMs. Furthermore, the *D*-/*G*-intensity ratio of GEPM samples increases with the increase in the amount of PEI, indicating that the introduction of PEI polymers has an obvious effect on the structure of GO sheets and results in increase of defects on both sides of GO sheets. The increase of defects in GEPMs can be accounted for slight reduction process of GO, consistent with the results reported elsewhere.[29,58]

The high porosity, remarkable nitrogen content, and mechanically stable graphene skeleton of the as-prepared GEPMs provide an ideal platform for the high-efficiency adsorption of dye. Figure 6a presents the adsorption curves of GEPM-1 toward two acidic dyes (amaranth and orange G) and one basic dye (rhodamine B). After 3 h, the removal of dye can basically reach equilibrium and a plateau was gradually formed thereafter. The total loading capacities of the GEPM-1 for amaranth and orange G were estimated to be 800 and 300 mg $g^{-1}$, respectively, which is higher than that of GEPM-1 for rhodamine B (25 mg $g^{-1}$). To the best of our knowledge, GEPM-1 exhibits the highest adsorption capacity for amaranth compared with other carbon materials such as powdered peanut hull (14.90 mg $g^{-1}$),[60] poly(ether sulfones)/poly(ethyleneimine) nanofibrous membrane (454.44 mg $g^{-1}$),[61] and mesoporous carbon (520 mg $g^{-1}$).[62] The high adsorption capacity of GEPM-1 for acidic dyes may mainly be attributed to the structure of GEPM-1: (1) the average pore diameter ($D_{pore}$) of GEPM-1 is 11.1 nm, which is large enough to facilitate the diffusion of dye; (2) the strong affinity of protonated amine groups toward the sulfonated groups of dye provides the driving force for the adsorption of acidic dye; (3) the porous structure of GEPM provides a large specific surface area and abundant conjugated domains of GO, which can greatly increase the contact opportunity of dye molecules on the GO sheets.[25]

The adsorption capacities of GEPMs for dyes increase with the introduction of PEI polymers (Figure 6b). For comparison, the adsorption capacities of pure GO powder for amaranth and orange G were calculated to be 11 and 7 mg $g^{-1}$, respectively. In addition, the kinetics parameters were analyzed using eq 2 and 3 and the linear plots are shown in Figure S4 (Supporting Information). From the correlation coefficients from eq 3 ($\gg$0.999), the adsorption process of GEPM-1 for dyes fit well with the pseudo-second-order kinetic model, which is consistent with these results reported preciously.[49,63] Furthermore, desorption behaviors of the loaded GEPM-1 were


dx.doi.org/10.1021/am402661t | ACS Appl. Mater. Interfaces 2013, 5, 9172–9179

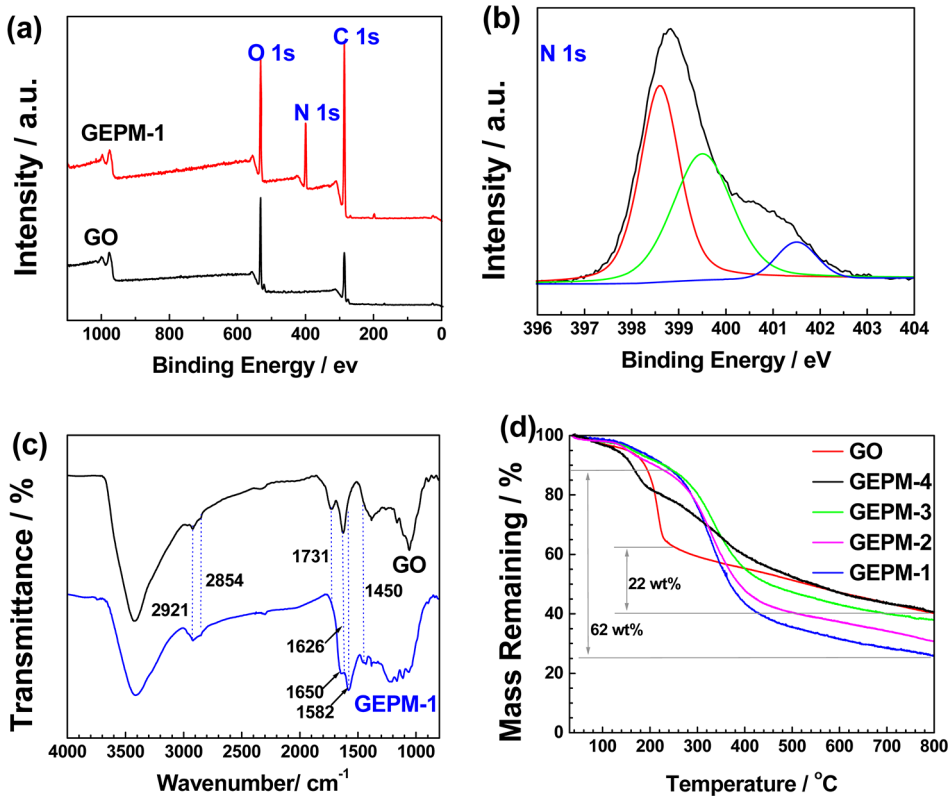


**Figure 4.** XPS survey spectra (a) and resolved nitrogen spectrum (b) of GO–PEI porous material (GEPM), IR spectra of GO and GEPM-1 (c), and TGA curves of GO and GEPMs obtained in nitrogen atmosphere (d).

**Scheme 1. Schematic Representation of GO–PEI Hydrogel**

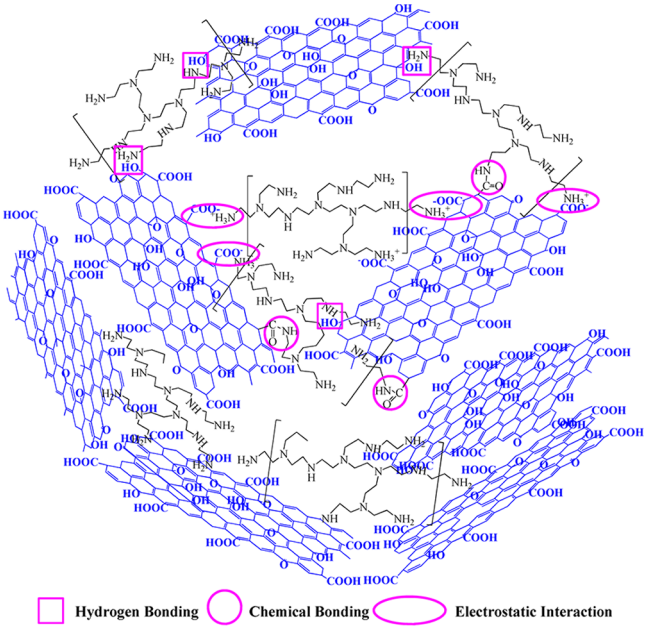


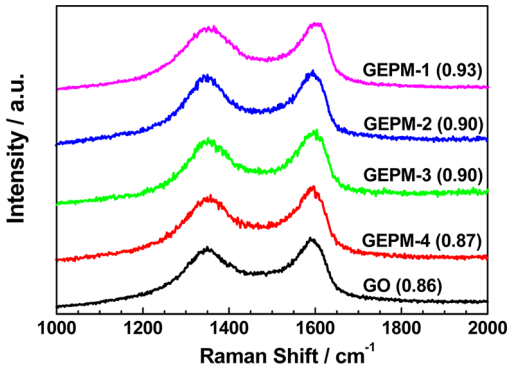


**Figure 5.** Raman spectra of GO and as-made GO–PEI porous materials (GEPMs). Numbers in the bracket represent for the *D*-/*G*-intensity ratio of the samples.

also studied as shown in Figure S5 (Supporting Information). It was found that CTAB is an excellent regenerant and the release percentage of the adsorbed dyes is approximately 69% and 72% for amaranth and orange G, respectively, which is close to that of graphene–CNT hybrid aerogels at the same condition (~70%).[49] Desorption process of the adsorbed dye molecules is probably attributed to strong interaction between CTAB and dye molecules. First, CTAB molecules possess the quaternary ammonium cations, which can strongly interact with sulfonic groups of dye molecules.[64,65] Second, the surfactant CTAB molecules form micelles in water and the adsorbed dyes can easily enter into the hydrophobic region of the micelles due to hydrophobic interaction between dye and CTAB. In addition, the surfactant CTAB could lower the interfacial tension between GO sheets and the dissolution medium (water), thus resulting in desorption of dye adsorbed.

Graphene and GO have been regarded as attractive candidate for gas adsorption due to their large surface area.[7,8] However, their adsorption capacity is limited as a result of the strong stacking of sheets.[66] The GEPMs can be considered as a novel kind of $CO_2$ adsorption material advantageously combining the unique 3D porous structure with high amine density to enhance the adsorption performance.


dx.doi.org/10.1021/am402661t | ACS Appl. Mater. Interfaces 2013, 5, 9172–9179

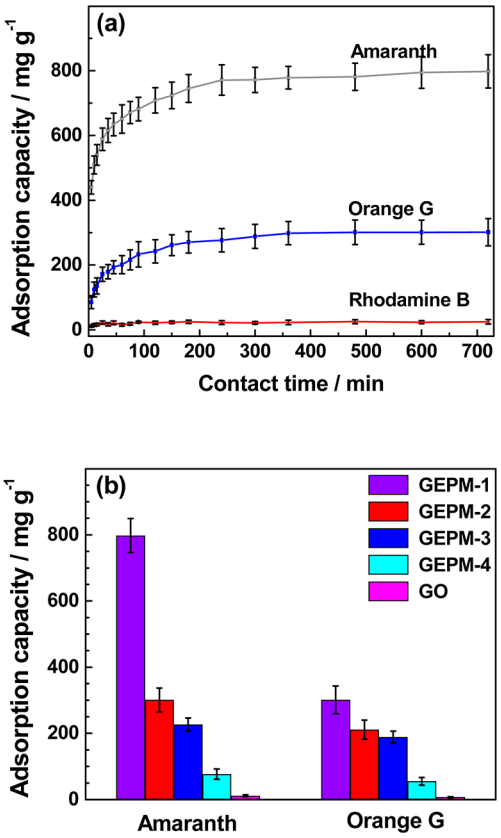


**Figure 6.** Adsorption curves of different dyes (amaranth, orange G, and rhodamine B) by GO–PEI porous material (GEPM) (a) and adsorption capacities of GEPMs for amaranth and orange G (b). For comparison, the related data collected with GO were also shown in (b).

As expected, GEPMs present high-performance adsorption behaviors for $CO_2$. $CO_2$ adsorption experiments were carried out at 273 K (Figure 7a and b). The $CO_2$ adsorption capacities of GEPM-1 show a maximum value of about 11 wt %, which is larger than HTG and GO samples and comparable to the carbon material reported previously at the same condition.[7,9,10] This may be owing to the interaction between the primary and secondary amino group in PEI and $CO_2$.[37,38] As shown in Figure 7a, the $CO_2$ adsorption isotherms of GO, HTG, and GEPM-1 show slight difference in the process of adsorption, which might be because of their different adsorption mechanism. The specific surface area and basic sites are two main factors to affect the $CO_2$ adsorption capacity. Although HTG has a large BET specific surface area (876 $m^2$ $g^{-1}$), it shows a lower adsorption capacity (8.1 wt %). The $CO_2$ adsorption isotherm is similar to those of other carbon materials and their adsorption capacity is mainly dependent on their surface area.[9,67] It is interesting that the uptake capacity for GO sample is close to 7.5 wt %; however, its BET specific surface area is only 31 $m^2$ $g^{-1}$. By fitting the $CO_2$ isotherm based on the Langmuir equation at 273 K, we found that GO has an estimated Langmuir surface area of 124 $m^2$ $g^{-1}$ (Figure S6, Supporting Information). The high uptake capacity of $CO_2$ on GO might be a result of the effect of surface heterogeneity.[68] Oxygen-containing functional groups could enhance the $CO_2$ adsorption in carbon materials. We are currently carrying out more detailed research to identify the relationship between $CO_2$ adsorption capacity and oxygenated functional groups of GO sheets. These results indicate the enhanced $CO_2$ adsorption performance of the GEPMs as a result of the introduction of basic sites and large specific surface area.

## CONCLUSIONS

In summary, we have successfully demonstrated a facile strategy for the preparation of 3D GO–PEI porous materials via the self-assembly of 2D GO sheets and PEI at room temperature under atmospheric pressure without stirring. The porous materials show a lightweight (0.02–0.03 g $cm^{-3}$), large BET specific surface area (476 $m^2$ $g^{-1}$), and hierarchically porous structure, offering great technological promise for a variety of applications. Furthermore, the as-prepared GEPMs show an excellent adsorption performance for amaranth (800 mg $g^{-1}$), which possess the highest adsorption capacity under the same condition compared with other carbon materials. In addition, the GEPMs also exhibit a good adsorption capacity for $CO_2$. This work indicates that the prepared GEPMs may find promising applications in environmental fields, such as the adsorption of waste dyes and the removal of greenhouse gas.

## ASSOCIATED CONTENT

### Supporting Information

Pore size distribution, kinetic curves of acidic dyes (amaranth and orange G), desorption curves of amaranth and orange G, and chemical structures of three dyes used in this study for the

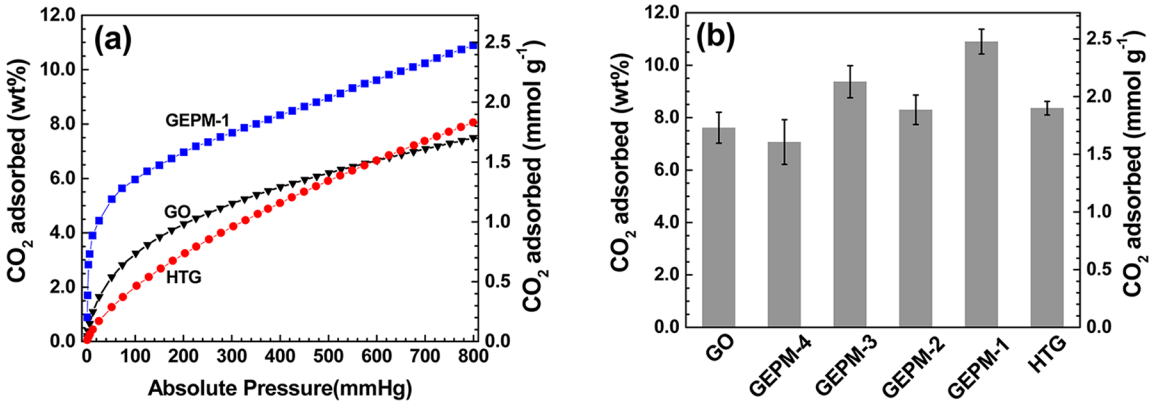


**Figure 7.** Carbon dioxide adsorption isotherms of GO, hydrothermal reduced graphene (HTG), and GO–PEI porous material (GEPM) samples (a) and capacity comparison of GO, HTG, and GEPMs (b).


dx.doi.org/10.1021/am402661t | ACS Appl. Mater. Interfaces 2013, 5, 9172–9179

GEPMs. This information is available free of charge via the Internet at http://pubs.acs.org/.

## AUTHOR INFORMATION


### Corresponding Author

*Tel: +86 10 8254 5576. E-mail: hanbh@nanoctr.cn.


### Notes

The authors declare no competing financial interest.

## ACKNOWLEDGMENTS

The financial support of the National Science Foundation of China (Grant 91023001), the Ministry of Science and Technology of China (Grant 2011CB932500), and the Chinese Academy of Science (Grant KJCX2-YW-H21) is acknowledged.

## REFERENCES


(1) Srinivas, G.; Zhu, Y.; Piner, R.; Skipper, N.; Ellerby, M.; Ruoff, R. *Carbon* **2010**, *48*, 630−635.
(2) Ma, L.-P.; Wu, Z.-S.; Li, J.; Wu, E.-D.; Ren, W.-C.; Cheng, H.-M. *Int. J. Hydrogen Energy* **2009**, *34*, 2329−2332.
(3) Ghosh, A.; Subrahmanyam, K. S.; Krishna, K. S.; Datta, S.; Govindaraj, A.; Pati, S. K.; Rao, C. N. R. *J. Phys. Chem. C* **2008**, *112*, 15704−15707.
(4) Dimitrakakis, G. K.; Tylianakis, E.; Froudakis, G. E. *Nano Lett.* **2008**, *8*, 3166−3170.
(5) Zhou, D.; Han, B.-H. *Adv. Funct. Mater.* **2010**, *20*, 2717−2722.
(6) Zhou, D.; Zhang, T.-L.; Han, B.-H. *Microporous Mesoporous Mater.* **2013**, *165*, 234−239.
(7) Burress, J. W.; Gadipelli, S.; Ford, J.; Simmons, J. M.; Zhou, W.; Yildirim, T. *Angew. Chem., Int. Ed.* **2010**, *49*, 8902−8904.
(8) Mishra, A. K.; Ramaprabhu, S. *AIP Adv.* **2011**, *1*, 032152.
(9) Srinivas, G.; Burress, J.; Yildirim, T. *Energy Environ. Sci.* **2012**, *5*, 6453−6459.
(10) Zhou, D.; Liu, Q.; Cheng, Q.-Y.; Zhao, Y.-C.; Cui, Y.; Wang, T.; Han, B.-H. *Chin. Sci. Bull.* **2012**, *57*, 3059−3064.
(11) Sun, Y.; Wu, Q.; Shi, G. *Energy Environ. Sci.* **2011**, *4*, 1113−1132.
(12) Chen, W. F.; Li, S. R.; Chen, C. H.; Yan, L. F. *Adv. Mater.* **2011**, *23*, 5679−5683.
(13) Eda, G.; Chhowalla, M. *Adv. Mater.* **2010**, *22*, 2392−2415.
(14) Xu, Z.; Zhang, Y.; Li, P. G.; Gao, C. *ACS Nano* **2012**, *6*, 7103−7113.
(15) Yao, P.; Chen, P.; Jiang, L.; Zhao, H.; Zhu, H.; Zhou, D.; Hu, W.; Han, B.-H.; Liu, M. *Adv. Mater.* **2010**, *22*, 5008−5012.
(16) Zhou, D.; Cui, Y.; Han, B.-H. *Chin. Sci. Bull.* **2012**, *57*, 2983−2994.
(17) Dreyer, D. R.; Park, S.; Bielawski, C. W.; Ruoff, R. S. *Chem. Soc. Rev.* **2010**, *39*, 228−240.
(18) Xu, B.; Yue, S. F.; Sui, Z. Y.; Zhang, X. T.; Hou, S. S.; Cao, G. P.; Yang, Y. S. *Energy Environ. Sci.* **2011**, *4*, 2826−2830.
(19) Mi, X.; Huang, G. B.; Xie, W. S.; Wang, W.; Liu, Y.; Gao, J. P. *Carbon* **2012**, *50*, 4856−4864.
(20) Srinivas, G.; Burress, J. W.; Ford, J.; Yildirim, T. *J. Mater. Chem.* **2011**, *21*, 11323−11329.
(21) Wu, D. Q.; Zhang, F.; Liang, H. W.; Feng, X. L. *Chem. Soc. Rev.* **2012**, *41*, 6160−6177.
(22) Xu, Y. X.; Sheng, K. X.; Li, C.; Shi, G. Q. *ACS Nano* **2010**, *4*, 4324−4330.
(23) Worsley, M. A.; Pauzauskie, P. J.; Olson, T. Y.; Biener, J.; Satcher, J. H.; Baumann, T. F. *J. Am. Chem. Soc.* **2010**, *132*, 14067−14069.
(24) Zhao, Y.; Hu, C. G.; Hu, Y.; Cheng, H. H.; Shi, G. Q.; Qu, L.-T. *Angew. Chem., Int. Ed.* **2012**, *51*, 11371−11375.
(25) Xu, Y. X.; Wu, Q. O.; Sun, Y. Q.; Bai, H.; Shi, G. Q. *ACS Nano* **2010**, *4*, 7358−7362.
(26) Jiang, X.; Ma, Y.; Li, J.; Fan, Q.; Huang, W. *J. Phys. Chem. C* **2010**, *114*, 22462−22465.
(27) Tang, Z.; Shen, S.; Zhuang, J.; Wang, X. *Angew. Chem., Int. Ed.* **2010**, *49*, 4603−4607.
(28) Bai, H.; Li, C.; Wang, X. L.; Shi, G. Q. *J. Phys. Chem. C* **2011**, *115*, 5545−5551.
(29) Huang, H.; Lu, S. Y.; Zhang, X. T.; Shao, Z. Q. *Soft Matter* **2012**, *8*, 4609−4615.
(30) Cheng, Q.-Y.; Zhou, D.; Gao, Y.; Chen, Q.; Zhang, Z.; Han, B.-H. *Langmuir* **2012**, *28*, 3005−3010.
(31) Sahu, A.; Choi, W. I.; Tae, G. *Chem. Commun.* **2012**, *48*, 5820−5822.
(32) Chen, C.; Yang, S.-T.; Ahn, W.-S.; Ryoo, R. *Chem. Commun.* **2009**, 3627−3629.
(33) Wang, X.; Schwartz, V.; Clark, J. C.; Ma, X.; Overbury, S.-H.; Xu, X.; Song, C. *J. Phys. Chem. C* **2009**, *113*, 7260−7268.
(34) Kassab, H.; Maksoud, M.; Aguado, S.; Pera-Titus, M.; Albela, B.; Bonneviot, L. *RSC Adv.* **2012**, *2*, 2508−2516.
(35) Li, P.; Ge, B.; Zhang, S.; Chen, S.; Zhang, Q.; Zhao, Y. *Langmuir* **2008**, *24*, 6567−6574.
(36) Zhao, J.; Simeon, F.; Wang, Y.; Luo, G.; Hatton, T.-A. *RSC Adv.* **2012**, *2*, 6509−6519.
(37) Goeppert, A.; Czaun, M.; May, R. B.; Prakash, G. K.; Olah, G. A.; Narayanan, S. R. *J. Am. Chem. Soc.* **2011**, *133*, 20164−20167.
(38) Kuwahara, Y.; Kang, D. Y.; Copeland, J. R.; Brunelli, N. A.; Didas, S. A.; Bollini, P.; Sievers, C.; Kamegawa, T.; Yamashita, H.; Jones, C. W. *J. Am. Chem. Soc.* **2012**, *134*, 10757−10760.
(39) Rezaei, F.; Lively, R. P.; Labreche, Y.; Chen, G.; Fan, Y. F.; Koros, W. J.; Jones, C. W. *ACS Appl. Mater. Interfaces* **2013**, *5*, 3921−3931.
(40) Labreche, Y.; Lively, R. P.; Rezaei, F.; Chen, G.; Jones, C. W.; Koros, W. J. *Chem. Eng. J.* **2013**, *221*, 166−175.
(41) Rosenholm, J. M.; Duchanoy, A.; Lindén, M. *Chem. Mater.* **2008**, *20*, 1126−1133.
(42) Hummers, W. S.; Offeman, R. E. *J. Am. Chem. Soc.* **1958**, *80*, 1339−1339.
(43) Zu, S.-Z.; Han, B.-H. *J. Phys. Chem. C* **2009**, *113*, 13651−13657.
(44) Cui, Y.; Wang, T.; Zhou, D.; Cheng, Q.-Y.; Zhang, C.-S.; Sun, S.-Q.; Liu, W.; Han, B.-H. *J. Phys. Chem. C* **2012**, *116*, 17698−17704.
(45) Wu, C.; Cheng, Q.-Y.; Sun, S.; Han, B.-H. *Carbon* **2012**, *50*, 1083−1089.
(46) Xu, J.; Wang, K.; Zu, S.-Z.; Han, B.-H.; Wei, Z. *ACS Nano* **2010**, *4*, 5019−5026.
(47) Zhang, D.-D.; Zu, S.-Z.; Han, B.-H. *Carbon* **2009**, *47*, 2993−3000.
(48) Zhang, X. T.; Sui, Z. Y.; Xu, B.; Yue, S. F.; Luo, Y. J.; Zhan, W. C.; Liu, B. *J. Mater. Chem.* **2011**, *21*, 6494−6497.
(49) Sui, Z. Y.; Meng, Q. H.; Zhang, X. T.; Ma, R.; Cao, B. *J. Mater. Chem.* **2012**, *22*, 8767−8771.
(50) Worsley, M. A.; Olson, T. Y.; Lee, J. R.; Willey, T. M.; Nielsen, M. H.; Roberts, S. K.; Pauzauskie, P. J.; Biener, J.; Satcher, J. H.; Baumann, T. F. *J. Phys. Chem. Lett.* **2011**, *2*, 921−925.
(51) Xu, C.; Wang, X.; Zhu, J. *J. Phys. Chem. C* **2008**, *112*, 19841−19845.
(52) Cai, D.; Song, M. *J. Mater. Chem.* **2007**, *17*, 3678−3680.
(53) Hu, H.; Zhao, Z. B.; Wan, W.; Gogotsi, Y.; Qiu, J. *Adv. Mater.* **2013**, *25*, 2219−2223.
(54) Zhou, X.; Chen, Z.; Yan, D.; Lu, H. *J. Mater. Chem.* **2012**, *22*, 13506−13516.
(55) Ren, T.; Li, L.; Cai, X.; Dong, H.; Liu, S.; Li, Y. *Polym. Chem.* **2012**, *3*, 2561−2569.
(56) Zhang, Y.; Chen, B.; Zhang, L.; Huang, J.; Chen, F.; Yang, Z.; Yao, J.; Zhang, Z. *Nanoscale* **2011**, *3*, 1446−1450.
(57) Sui, Z. Y.; Zhang, X. T.; Lei, Y.; Luo, Y. J. *Carbon* **2011**, *49*, 4314−4321.
(58) Zhou, D.; Cheng, Q.-Y.; Han, B.-H. *Carbon* **2011**, *49*, 3920−3927.
(59) Zhang, Z.; Ma, X.; Wang, D.; Song, C.; Wang, Y. *AlChE J.* **2012**, *58*, 2495−2502.
(60) Gong, R. M.; Ding, Y.; Lie, M.; Yang, C.; Liu, H. J.; Sun, Y. Z. *Dyes Pigm.* **2005**, *64*, 187−192.

(61) Min, M. H.; Shen, L. D.; Hong, G. S.; Zhu, M. F.; Zhang, Y.; Wang, X. F.; Chen, Y. M.; Hsiao, B. S. *Chem. Eng. J.* **2012**, *197*, 88−100.
(62) Li, J. T.; Li, B. L.; Wang, H. C.; Bian, X. B.; Wang, X. M. *Carbon* **2011**, *49*, 1912−1918.
(63) Sun, L.; Tian, C.; Wang, L.; Zou, J.; Mu, G.; Fu, H. *J. Mater. Chem.* **2011**, *21*, 7232−7239.
(64) Guo, J.; Chen, S.; Liu, L.; Li, B.; Yang, P.; Zhang, L.; Feng, Y. *J. Colloid Interface Sci.* **2012**, *382*, 61−66.
(65) Ansari, R.; Seyghali, B.; Mohammad-Khah, A.; Zanjanchi, M. A. *J. Surfactants Deterg.* **2012**, *15*, 557−565.
(66) Zhao, Y. X.; Ding, H. L.; Zhong, Q. *Appl. Surf. Sci.* **2012**, *258*, 4301−4307.
(67) Chandra, V.; Yu, S. U.; Kim, S. H.; Yoon, Y. S.; Kim, D. Y.; Kwon, A. H.; Meyyappan, M.; Kim, K. S. *Chem. Commun.* **2012**, *48*, 735−737.
(68) Liu, Y. Y.; Wilcox, J. *Environ. Sci. Technol.* **2012**, *46*, 1940−1947.